Joint Electromagnetic and Gravitational Wave Inference of Binary Neutron Star Merger GW170817 Using Forward-Modeling Ejecta Predictions

Marko Ristić [●],[1, 2, *] Richard O'Shaughnessy [●],[3] Kate Wagner [●],[3] Christopher J. Fontes [●],[1, 4]
Chris L. Fryer [●],[1, 5, 6, 7, 8] Oleg Korobkin [●],[1, 2] Matthew R. Mumpower [●],[1, 2] and Ryan T. Wollaeger [●][1, 5]

[1]*Center for Theoretical Astrophysics, Los Alamos National Laboratory, Los Alamos, NM 87545, USA*
[2]*Theoretical Division, Los Alamos National Laboratory, Los Alamos, NM 87545, USA*
[3]*Center for Computational Relativity and Gravitation, Rochester Institute of Technology, Rochester, New York 14623, USA*
[4]*Computational Physics Division, Los Alamos National Laboratory, Los Alamos, NM, 87545, USA*
[5]*Computer, Computational, and Statistical Sciences Division, Los Alamos National Laboratory, Los Alamos, NM 87545, USA*
[6]*The University of Arizona, Tucson, AZ 85721, USA*
[7]*Department of Physics and Astronomy, The University of New Mexico, Albuquerque, NM 87131, USA*
[8]*The George Washington University, Washington, DC 20052, USA*
(Dated: March 18, 2025)

We reassess the capacity for multimessenger inference of AT2017gfo/GW170817 using both kilonova and gravitational wave emission within the context of a recent simulation-based surrogate model for kilonova emission. Independent of the inclusion of gravitational wave observations, comparisons between observations that incorporate our kilonova model favor a narrow range of ejecta properties, even when allowing for a wide range of systematic uncertainties in our modeling approach. Conversely, we find that astrophysical conclusions about the neutron star itself, including its mass and radius, depend strongly on assumptions about how much material is ejected from the neutron star. Looking forward, our analysis highlights the importance of systematic uncertainty in general, the need for better modeling of neutron star merger mass ejection from first principles, and warns against uncontextualized applications of ejecta predictions using fits to numerical relativity simulations.

I. INTRODUCTION

The detection of gravitational waves (GWs) emitted by binary neutron star (BNS) merger GW170817 [1, 2] and, subsequently, electromagnetic (EM) radiation from its associated counterpart AT2017gfo [3–19] introduced exciting prospects for studying the universe using multimessenger astronomy. The GWs emitted by BNS mergers carry information about the pre-merger binary, such as the masses, spins, and tidal deformabilities of the merging neutron stars. Likewise, the EM radiation from the counterpart, or "kilonova" [20, 21], conveys details about the material that was ejected during and after the merger [22], tying directly to the fate of the merger remnant [23–25], the dense matter equation of state (EOS) [26, 27], and r-process nucleosynthesis [28–30].

Following the GW170817/AT2017gfo detection, recent studies have performed numerous numerical relativity simulations of binary neutron star mergers (e.g. [31–44]). Using these simulations, certain studies identified fitting formulae that connect ejecta properties to the parameters of the binary that are easily extractable from the GW signal [45–47]. These fits have been used in previous multimessenger analyses to place stronger constraints on unknown quantities like the EOS [46, 48, 49], particularly in the case of GW190425, a black-hole-neutron-star merger whose ejected mass had to be inferred using one of these fits due to the lack of an electromagnetic counterpart [50].

Previous work has identified that these fits to numerical relativity simulations exhibit variable validity in different regions of binary parameter space [51]. Moreover, the underlying simulations used to build these fits only cover a very limited range of possible binary merger configurations. Nonetheless, as we will demonstrate in this work, large-scale multimessenger inference calculations must employ these fits far outside the regions in which they have been calibrated. The need for using these fits outside of their safely-calibrated region has not been emphasized in the many previous studies that have employed them (e.g. [49]).

Motivated by a recently developed surrogate model for kilonova emission that provides the most constraining ejecta information to date [52], in conjunction with previous studies examining the agreement between ejecta fits (e.g. [51]), in this study we examine how these ejecta fits inform multimessenger inference of the binary parameters. We emphasize that our kilonova model is by no means complete in the sense that many systematic uncertainties are still omitted. Recent studies have identified multiple additional sources of systematic uncertainty along the merger-to-kilonova modeling chain [53–55]. Nevertheless, our surrogate model's ability to tightly constrain ejecta parameters enables us to investigate the systematic uncertainties that propagate into Bayesian inference analyses that utilize these fits. Our intent with this study is to highlight the systematic uncertainties that are propagated when using these fits for more informed use in future studies.

The paper is structured as follows. Section II outlines our methodology, including details about the numerical

relativity ejecta fits, our kilonova surrogate model and the simulations on which it is based, and our Bayesian inference approach. In Section III, we discuss the results of our analysis, specifically focusing on the cases where the fraction of the accretion disk unbound as ejecta is treated as a free versus fixed parameter. In Section IV, we discuss our results and the implications of our findings. Finally, we conclude the paper in Section V.

II. METHODOLOGY

At a high level, our methodology proceeds as follows: we generate iterative grids of samples across our binary parameter space over which the likelihood is evaluated. For the GW data, we perform a coordinate transformation of our binary parameters to $\mathcal{M}_c$ (chirp mass), q (mass ratio), $\tilde{\Lambda}$ (effective tidal deformability), and χ_{eff} (effective spin) and calculate the GW likelihood through comparison to the GW170817 waveform. For the EM data, we calculate the ejecta properties from the binary parameter samples using the ejecta fits, create light curves corresponding to these ejecta properties, and calculate the EM likelihood through comparison to the AT2017gfo light curves. We continue generating iterative sample grids, informed by the prior iteration's likelihood, until we reach convergence ($\mathcal{O}(1000)$ effective samples).

A. Ejecta fits to numerical relativity simulations

We employ the forward model ejecta fits from Refs. [45–47], hereafter referred to as KruFo20, DiCo20, and Nedora21, respectively. These fits to numerical relativity simulations estimate the ejecta properties, namely dynamical and wind ejecta mass and velocity, given binary properties (mass ratio q and neutron star radius $R_{1.4}$) as inputs. In summary, KruFo20 present fitting formulae based on 52 numerical relativity simulations of binary neutron star mergers compiled from Refs. [33] and [34]. DiCo20 base their formulae on 73 numerical relativity simulations, using the two aforementioned sources in addition to simulations from Refs. [32] and [31]. Finally, Nedora21 employs the largest numerical relativity dataset to date for their fits, using 324 models from Refs. [32–44]. The implementation of these ejecta fits follows the approach outlined in Section II.F of Ref. [56], with the exception of the modifications described in this section.

Each ejecta fit predicts the ejecta mass, ejecta velocity, and accretion disk mass as a function of the binary mass ratio q and the neutron star radius $R_{1.4}$. In none of the ejecta fit models is there a prescription for tying the disk mass to post-merger wind mass; instead, we map the fits' ejecta mass prediction to the dynamical ejecta, and assume some fraction f_{disk} of the disk mass is ejecta as wind ejecta. In Figure 1, we display naive contours corresponding to representative values of these ejecta param-
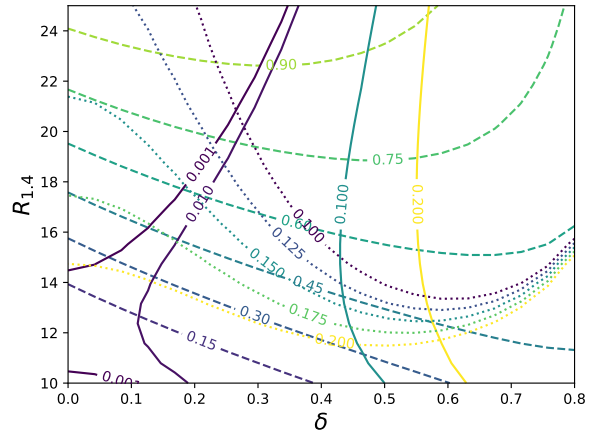

FIG. 1. Solid, dashed, and dotted line contours corresponding to the KruFo20 dynamical ejecta mass m_{ej}, disk mass m_{disk}, and ejecta velocity v_{ej}, respectively. Contours were calculated as a function of mass ratio $\delta = (m_1 - m_2)/(m_1 + m_2)$ and neutron star radius $R_{1.4}$. Mass and velocity units are in $M_{\odot}$ and c, respectively.

eters as a function of the binary parameters, fixing the binary source-frame chirp mass to the observed value for GW170817. The solid, dashed, and dotted lines indicate $m_{\mathrm{ej}}(\delta, R_{1.4})$, $m_{\mathrm{disk}}(\delta, R_{1.4})$, and $v_{\mathrm{ej}}(\delta, R_{1.4})$, respectively. The solid dynamical ejecta contours constrain the mass ratio q while allowing for a broad range of radii. Conversely, the dashed disk mass contours constrain $R_{1.4}$ to favor low values for realistic disk masses with a slight constraint on δ. Critically, however, the dotted v_{ej} contours – shown at levels corresponding to our previously-inferred estimate for this quantity – exclude the conventional interpretation for GW170817, which consists of $\delta \simeq 0$ (comparable masses) and $R_{1.4} \simeq 12$km. Instead, the v_{ej} contours follow a trendline that permits either comparable mass but large radius or conventional radius but highly asymmetric masses, both scenarios that could produce sufficiently low dynamical ejecta velocities in binary neutron star mergers.

Because electromagnetic observations constrain these three ejecta properties independently (by way of kilonova models which introduce their own systematic uncertainties), only in exceptional circumstances can all three equations be solved simultaneously for a self-consistent pair of binary properties ($\delta, R_{1.4}$: we have more equations than unknowns). However, the ejecta parameters preferred by our previous analyses, notably and critically the ejecta velocity, are at or beyond the range of underlying simulation data used to train these analytic approximate fits. As a result, motivated by previous work, we generously allow for independent systematic uncertainty in all three predictions for ejecta properties.

Rather than estimating the uncertainties on the ejected mass from each of our two components, we assign free parameters α_{dyn} and f_{disk} to quantify these systematic un-

certainties during inference. The $\alpha_{\rm dyn}$ parameter serves as a scale factor for the fits' dynamical ejecta mass prediction, while $f_{\rm disk}$ dictates what fraction of the accretion disk is expelled as wind ejecta. Given the behavior of the dotted $v_{\rm ej}$ contours in Figure 1, we also include a systematic uncertainty parameter for the ejecta velocity, β_ϕ. To uniformly explore the systematic uncertainty in velocity space, we apply the reparameterization $\phi = \ln((c/v)^2 - 1)$. Our uncertainty is characterized by a uniformly distributed random variable β_ϕ added to ϕ.

The ejecta fits predict a total ejecta velocity v_{ej} by adding in quadrature the velocities describing the ejecta within and perpendicular to the orbital plane, without explicitly declaring to which of the dynamical and wind components that ejecta belongs (see Eqs. (5)–(9) in Ref. [57]). In this study, following previous conventions (e.g. [58]), we set the dynamical ejecta velocity to the value calculated only for the perpendicular velocity component such that $v_d = v_z$ and fix the wind velocity $v_w = 0.10c$ per the results of our previous analysis in Ref. [52]. This choice is similar to previous approaches, e.g. as in Ref. [56], where the wind velocity v_w was set to $0.08c$ as informed by Ref. [33].

The employed fits also have a lower limit on the accretion disk mass of $\log M_{\rm disk} \geq -3$, but no defined upper limit. As certain combinations explored during sampling may yield binary parameters outside of the realm of validity for the ejecta fits, we set an associated restriction on the wind mass such that $\log m_w \leq -1$.

B. Kilonova simulations and surrogate model

We assume a two-component kilonova model consisting of lanthanide-rich, equatorial dynamical ejecta and lanthanide-poor, axial wind ejecta as described in [59, 60] and motivated by numerical simulations [22, 61]. Each component is assumed to be homologously expanding and parameterized by a mass and velocity such that $M_{\rm d}$, $v_{\rm d}$ and $M_{\rm w}$, $v_{\rm w}$ describe the dynamical and wind components' masses and averaged velocities, respectively. The morphology for the dynamical component is an equatorially centered torus, while the wind component is represented by an axially-centered peanut component; Figure 1 of [59] displays the torus-peanut, or "TP," schematic corresponding to the morphologies employed in this work; see Ref. [60] for a detailed definition.

The lanthanide-rich dynamical ejecta stems from r-process nucleosynthesis in the neutron-rich ejected material, characterized by a low electron fraction ($Y_{\rm e} \equiv n_{\rm p}/(n_{\rm p} + n_{\rm n})$) of $Y_e = 0.04$, with elements reaching the third r-process peak ($A \sim 195$). The wind ejecta originates from higher $Y_e = 0.27$ that encapsulates elements between the first ($A \sim 80$) and second ($A \sim 130$) r-process peaks. The detailed breakdown of the elements in each component can be found in Table 2 of Ref. [59].

To generate the simulations on which the surrogate model discussed in this work is trained, we use SuperNu

[62], a Monte Carlo code for simulation of time-dependent radiation transport with matter in local thermodynamic equilibrium. The simulated kilonova spectra $F_{\lambda,\rm sim}$ assume the aforementioned two-component model. Both components are assumed to have fixed composition and morphology for the duration of each simulation. SuperNu uses radioactive power sources calculated from decaying the r-process composition from the WinNet nuclear reaction network [63–66]. These radioactive heating contributions are also weighted by thermalization efficiencies introduced in Ref. [67] (see Ref. [68] for a detailed description of the adopted nuclear heating). We use detailed opacity calculations via the tabulated, binned opacities generated with the Los Alamos suite of atomic physics codes [69–71]. In the database that we use, the tabulated, binned opacities are not calculated for all elements; therefore, we produce opacities for representative proxy elements by combining pure-element opacities of nuclei with similar atomic properties [70]. Specifics of the representative elements for our composition are given in Ref. [59].

The SuperNu outputs are observing-angle-dependent, simulated spectra $F_{\lambda,\rm sim}$, post-processed to a source distance of 10 pc, in units of $\rm erg\,s^{-1}\,cm^{-2}\,\AA^{-1}$. The spectra are binned into 1024 equally log-spaced wavelength bins spanning $0.1 \leq \lambda \leq 12.8$ microns. For the purposes of this work, we consider the light curves for the 2MASS $grizy$ and Rubin Observatory JHK broadband filters. As we only consider anisotropic simulations in this study, unless otherwise noted, we extract simulated light curves using 54 angular bins, uniformly spaced in $\cos\theta$ over the range $-1 \leq \cos\theta \leq 1$. The angle θ is taken between the line of sight and the symmetry axis as defined in Equation (2) of Ref. [52], with further description of the treatment of observing angle found therein.

We interpolate over the library of SuperNu simulations described in [52, 72] using the multi-layer perceptron (MLP) described in [52]. In summary, the MLP was trained on ~ 250 light-curve simulations evaluated at 264 log-spaced times between 0.125 and 37.24 days for 54 viewing angles equally spaced in $\cos\theta$ for θ ranging from 0 to 180°. We do not perform any normalization of our inputs or outputs, with ejecta parameters ranging from $-3 \leq \log m/M_\odot \leq -1$ and $0.05 \leq v/c \leq 0.3$ and light curves ranging from -18 to 8 AB magnitudes. We train a separate MLP for each of our broadband filters, training each MLP for 1000 epochs with a batch size of 32 using the Adam optimizer. Our initial learning rate is 2×10^{-4} with a decay rate of 5% every 10 epochs.

C. The likelihood of ejecta parameters for AT2017gfo given electromagnetic observations

The AT2017gfo data is originally presented in [3–14, 16, 17, 19, 73, 74]. Each sample $\vec{x}_\theta$ is evaluated by the MLP to produce a light-curve prediction $\hat{y}$ for every one of the $grizyJHK$ broadband filters. We calcu-

late the residual between the MLP prediction $\hat{y}$ and the AT2017gfo observed data in time i for every band B by way of the reduced-χ^2 statistic

$$\chi^2 = \sum_{i,B} \frac{(\hat{y}_{i,B} - d_{i,B})^2}{\sigma_i^2 + \sigma_{\mathrm{sys}}^2}. \qquad (1)$$

In our χ^2 residual calculation, we include statistical uncertainties from the AT2017gfo data σ_i, as well as systematic uncertainties σ_{sys} which we use as a catch-all term to encompass all uncertainties, quantifiable or otherwise, associated with the neural network interpolation process and kilonova modeling uncertainties. Unlike in previous work (Ref. [52]), we set our systematic modeling uncertainty σ_{sys} as a free parameter to allow for easier reconciliation of the GW and EM inferences. We adopt a purely Gaussian likelihood based on these residuals, i.e.

$$\ln \mathcal{L} = -\frac{\chi^2}{2} - \frac{1}{2} \ln(2\pi)^N \sum_i (\sigma_i^2 + \sigma_{\mathrm{sys}}^2), \qquad (2)$$

where N is the total number of AT2017gfo observations.

D. The likelihood of source parameters for GW710817 given gravitational wave observations

Following previous studies that constrain properties of GW170817 and the equation of state from GW observations [75–78], we use the RIFT parameter inference engine [79–81] to explore and evaluate the marginal likelihood $L(x)$ for a wide range of different compact binary source parameters x. Following the RIFT paradigm, the parameters x include all intrinsic (detector-frame) quantities needed to phenomenologically characterize the binary's inspiral: its two component masses, spins, and tidal deformabilities, assumed independent of any specific EOS model. We then use standard nonparametric interpolation techniques (here, random forests from `sklearn`) to interpolate the marginal likelihood to provide a continuous estimate $\hat{L}(x)$.

To be more concrete, we will employ precisely the same analysis framework and settings as used in Ref. [82]. As a brief review to establish notation, gravitational wave observations of GW170817 constrain the binary masses m_i and tidal deformabilities Λ_i for each component i of the binary [1, 26, 75, 83]. The presence of matter impacts the binary's inspiral at leading order through each component's dimensionless tidal deformability parameter $\Lambda_i = (2/3)k_2(c^2 r_i / G m_i)^5$ [84], where k_2 is the $l = 2$ Love number, m_i is the neutron star mass, and r_i is the neutron star radius. The leading order contribution to the phase evolution of a GW inspiral is given by the weighted combination of Λ_i terms

$$\tilde{\Lambda} = \frac{16}{13} \frac{(m_1 + 12m_2)m_1^4 \Lambda_1 + (m_2 + 12m_1)m_2^4 \Lambda_2}{(m_1 + m_2)^5}. \qquad (3)$$

The impacts of tidal effects on outgoing radiation are included in many conventional approximate phenomenological estimates of outgoing radiation from merging compact binaries. In this work, we begin with precisely the marginal likelihood data accumulated in Ref. [82]. That investigation was performed with a contemporary state-of-the-art model, IMRPhenomPv2_NRTidalv2 [85, 86], which incorporates precession physics but omits higher-order modes. This analysis was performed with open GW data for GW170817 available from GWOSC [87], using the same power spectral densities provided with GWTC-1 [88, 89], over a frequency range from 23Hz to 1700Hz, with known sky location and source luminosity distance derived from the electromagnetically-identified host galaxy. For exploration purposes, most prior assumptions were customary (e.g., uniform in detector-frame component masses), noting that the previous investigation employed multiple spin priors and mass ratio priors to accumulate marginal likelihood information over a wide range of source parameters. Although this analysis included prior information about the alignment between the binary's angular momentum direction and the line of sight, inferred from late-time radio afterglow observation [90, 91], this information should not significantly impact intrinsic parameters.

Because the original marginal likelihood grid accumulated in Ref. [82] did not extend to cover all of the extreme BNS configurations needed in our study, we replicated and extended this analysis to ensure that marginal likelihood data was present whenever required for joint EM/GW analysis. For simplicity, we employ the same GW model throughout for all $\tilde{\Lambda}$, keeping in mind that this model was not calibrated over the full range of Λ that are needed to carry out our investigation.

Figure 2 shows the raw marginal GW likelihood data employed in our analysis, before continuous interpolation over binary neutron star parameters. We show the GW likelihood as a function of the chirp mass $\mathcal{M}_c = (m_1 m_2)^{3/5}/(m_1 + m_2)^{1/5}$, mass ratio $q = m_2/m_1$, effective spin $\chi_{\mathrm{eff}} = (a_{1\mathrm{z}} + q a_{2\mathrm{z}})/(1 + q)$, and effective tidal deformability $\tilde{\Lambda}$ as defined in Equation 3. In this figure, the color indicates the marginal likelihood, scaling from higher (white) to lower (black) likelihood values, with gray points showing values below the $\ln \mathcal{L}_{\mathrm{max}} - 15$ cutoff. This figure highlights the broad coverage of our underlying likelihood data, particularly the wide range of $\tilde{\Lambda}$. Our coverage includes carefully assessing the marginal likelihood of GW signals in many regions far outside the customary GW posterior, which is concentrated in the white region. To put our broad exploration in context, drawing upon analyses to be discussed in detail in Section III A, in this figure we also show the results of three joint GW+EM inferences, using the DiCo20 (red), KruFo20 (black), and Nedora21 (blue) ejecta fits, respectively. As described later, all three analyses adopt conventional spin and mass ratio priors, consistent with previously published interpretations using comparable models, settings, and data [1, 75]. Nonetheless, our joint GW+EM in-
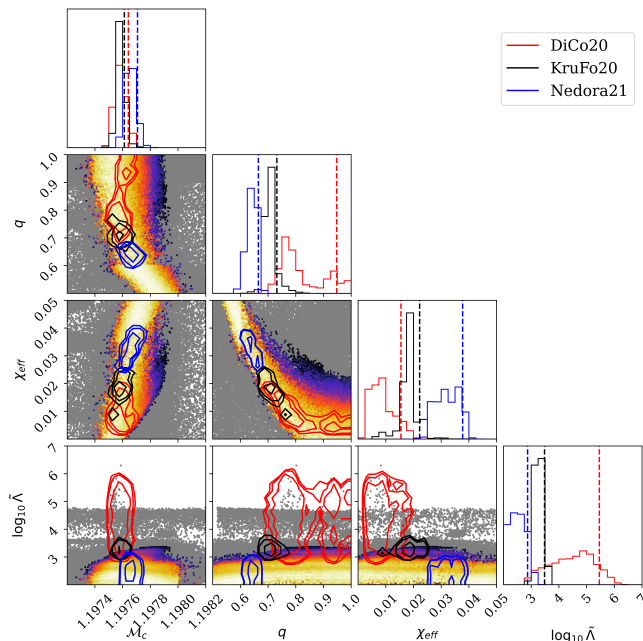
FIG. 2. In this figure, the colored dots represent the input marginal likelihood data assumed in our analysis. In black, red, and blue, we overplot posteriors corresponding to the 90% credible interval for the KruFo20, DiCo20, and Nedora21 GW+EM predictions, respectively. Here, $\mathcal{M}_c$ is in the detector frame.

E. Bayesian inference

We use the RIFT framework [92] to adaptively perform Monte Carlo integration and generate samples. As previously, we employ an adaptive volume Monte Carlo integrator, following closely the approach outlined in Ref. [93]. The adaptive volume integrator allows for more efficient sampling given the higher-dimensional space explored in this work. As our inference is performed via adaptive Monte Carlo integration, the reliability of our posterior can be expressed in terms of a number of effective samples $n_{\rm eff}$. Several different conventions exist for this number; see the appendix of Ref. [81] for more detailed discussion. For this study, we terminate our analyses when $n_{\rm eff} \simeq 10^3$, indicating sufficient convergence.

Table I shows the sampling parameters used during inference, along with their associated lower and upper limits and priors. The combination of the chirp mass $\mathcal{M}_c$ and mass asymmetry δ priors provide an equivalent locally uniform prior for the binary masses m_1 and m_2. In addition to the masses, we also sample for the spins of the neutron stars $s_{1\rm z}$ and $s_{2\rm z}$. We assume that both of the neutron stars have the same radius given a 1.4 $M_\odot$ neutron star $R_{1.4}$, treating this radius as a proxy for the nuclear EOS. As described in Sec. II A, we introduce parameters $\alpha_{\rm dyn}$ and $f_{\rm disk}$ that encapsulate the uncertainty in our ejected dynamical and wind mass, respectively. These parameters are sampled in addition to the light-curve systematics $\sigma_{\rm sys}$, effectively allowing for three separate measures of systematic uncertainty in our analysis. Finally, we sample for the viewing angle θ as in prior work (e.g. Ref. [52]). All parameters in Table I are assumed to be dimensionless unless their names are followed by units in brackets.

Parameter	Limits	Prior
$\mathcal{M}_c$ [$M_\odot$]	[1.1855, 1.1865]	Jointly uniform m_1, m_2
δ	[0, 0.5]	Jointly uniform m_1, m_2
$s_{1\rm z}$	[0, 0.05]	Uniform
$s_{2\rm z}$	[0, 0.05]	Uniform
$R_{1.4}$ [km]	[8, 25]	Uniform
$\log \alpha_{\rm dyn}$	[−5, 2]	Uniform
$\log f_{\rm disk}$	[−5, 0]	Uniform
β_ϕ	[−2, 2]	Uniform
$\sigma_{\rm sys}$	[0, 8]	Uniform
θ [deg]	[0, 90]	$\mathcal{N}(\mu = 20, \sigma = 5)$

TABLE I. Sampling parameters along with their associated limits and priors. Parameters are dimensionless unless units in brackets are specified in the parameter column. The priors in $\mathcal{M}_c$ and δ are equivalent to a locally uniform probability density in m_1, m_2.

ferences favor more extreme binary and/or tidal parameters compared to previously reported posterior inferences using GW alone, including asymmetric mass ratio (all except DiCo20), large tidal deformability (KruFo20 and DiCo20), and sometimes even large spin (Nedora21). As these extreme configurations are not well-represented in widely-used fiducial posterior samples from the original analyses, previous follow-up GW+EM investigations that rely on simply reweighting these fiducial samples will not fully capture the features that we report below. In other words, our subsequent calculations demand the wide-ranging likelihood-based approach adopted here.

III. RESULTS

A. All systematics included ($\alpha_{\rm dyn}, f_{\rm disk}, \beta_\phi$)

We verify that our ejecta fit posteriors produce consistent kilonova ejecta properties in Figure 3. For all the analyses in this section, we assume that both the systematic uncertainty on the ejecta velocity and the fraction of the disk $f_{\rm disk}$ representing the amount of ejected wind mass are treated as free parameters. Light-curve systematic uncertainty $\sigma_{\rm sys}$ is treated as a free parameter for all analyses in this manuscript. We begin by examining the posteriors for the binary's ejecta properties, primarily constrained by our EM likelihood $\mathcal{L}_{\rm EM}$. Figure 3 shows the predicted ejected masses, bulk velocity (attributed to the dynamical ejecta), and the viewing angle derived from the inferences presented in Figure 5. In this analysis, we adopt $v_w = 0.10c$, consistent with numerical
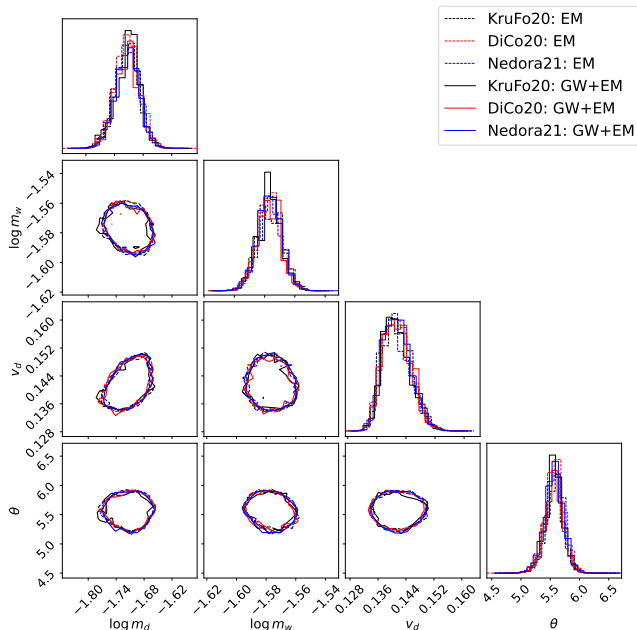
FIG. 3. Ejecta posterior distributions using EM (dashed) and GW+EM (solid) likelihoods with the disk mass ejection fraction left as a free parameter. The wind velocity is fixed to $v_w = 0.10c$ per the posteriors in Ref. [52]. There is little difference in the ejecta posteriors between the two approaches, modulo artifacts from varying sample counts, due to our kilonova model requiring parameters in a very narrow region to recreate the AT2017gfo light curves. Figure 5 highlights the differences in the binary parameters when including the GW likelihood.

simulations and our previous analysis of AT2017gfo [52]. The dashed black, red, and blue lines correspond to inferences using only AT2017gfo data $\mathcal{L}_{\mathrm{EM}}$ for the KruFo20 DiCo20 and Nedora21 ejecta fits, respectively. The solid lines show the same analysis when incorporating both the AT2017gfo $\mathcal{L}_{\mathrm{EM}}$ and GW170817 $\mathcal{L}_{\mathrm{GW}}$ data. Due to considerable flexibility in ejecta mass model systematics (i.e., $f_{\mathrm{disk}}, \alpha_{\mathrm{dyn}}$), our model recovers once again a nearly indistinguishable distribution of ejecta parameters. Since our inference tries to fit AT2017gfo observations with our model, and since our ejecta model allows for systematic error, our inferences always find consistent solutions for the best-fitting ejecta, i.e. the ejecta parameters that consistently explain AT2017gfo within the context of our kilonova model family, subject to the limitations of those kilonova models. The much larger and more rapidly varying electromagnetic likelihood dominates our inference of these ejecta properties. By contrast, the GW information only slightly perturbs the overall conclusions obtained electromagnetically. The inclusion of an ejecta velocity model systematic parameter does not affect the similarity of the ejecta posteriors.

In Figure 4, we plot the light curves associated with the Nedora21 GW+EM posteriors from Figure 3, showing both the mean and posterior 68% credible interval.

The width of these posterior intervals derives from and reflects the narrow posteriors shown in Figure 3 (including suppressed parameters reflecting model systematic uncertainty). As in previous studies (e.g. [72, 94]), we observe residual model systematics relative to the data, where the largest deviations between our models and the data occur in the bluer filters, namely the g and r bands, starting at ~ 3 days. Though we explore possible reasons for this blue filter discrepancy in prior work (see Figure 2 of [72]), we do not explicitly include this model fidelity issue in our formulation of σ_{sys}. Both in this work, where we treat σ_{sys} as a free parameter, and in our previous EM-only inferences, where we assume $\sigma_{\mathrm{sys}} = 0.5$ [52, 72, 95], the deviations that would arise from variations in the posteriors are well-encompassed by our systematics. Thus, for all intents and purposes, we expect the slight deviations of the posteriors in Figure 3 to have negligible effects on our findings.
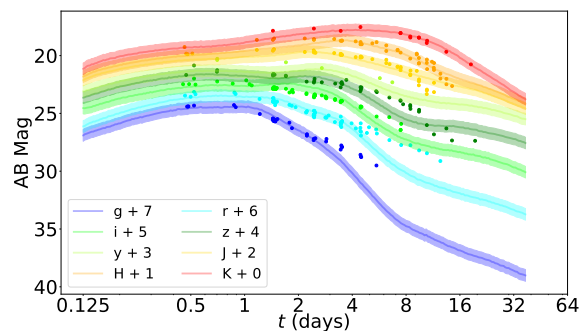

FIG. 4. Light curves predicted by our kilonova surrogate model for the Nedora21 GW+EM ejecta posteriors presented in Figure 3, with solid lines corresponding to the median posterior values and shaded bands representing 1σ uncertainty. This posterior includes the effect of marginalizing over unknown model systematic uncertainty σ_{sys}, as described in the text.

The corner plots in Figure 5 show 90% two-dimensional credible intervals and one-dimensional marginal posterior distributions for the underlying binary (m_c, δ), EOS $(R_{1.4})$, and ejecta systematic $(f_{disk}, \alpha_{dyn}, \beta_\phi)$ model parameters. As in Figure 3, the dashed curves represent inference using data from AT2017gfo alone and the solid curves consider both the AT2017gfo and GW170817 data. We do not plot the posteriors for s_{1z}, s_{2z}, and σ_{sys} as they are largely uninteresting in the context of understanding the ejecta fits and would have reduced the legibility of Figure 5. Following a preliminary analysis to identify the posterior support for each ejecta fit, we perform focused analyses targeting narrow regions of f_{disk} for each ejecta fit: $\log f_{\mathrm{disk}}$ is uniform over [-0.9, -0.75], [-1.4, -1.2], and [-1.2, -1] for DiCo20, KruFo20, and Nedora21, respectively.

As expected, our analysis finds that the three ejecta models can only explain AT2017gfo using dramatically different progenitor binaries and EOS. Two of the three
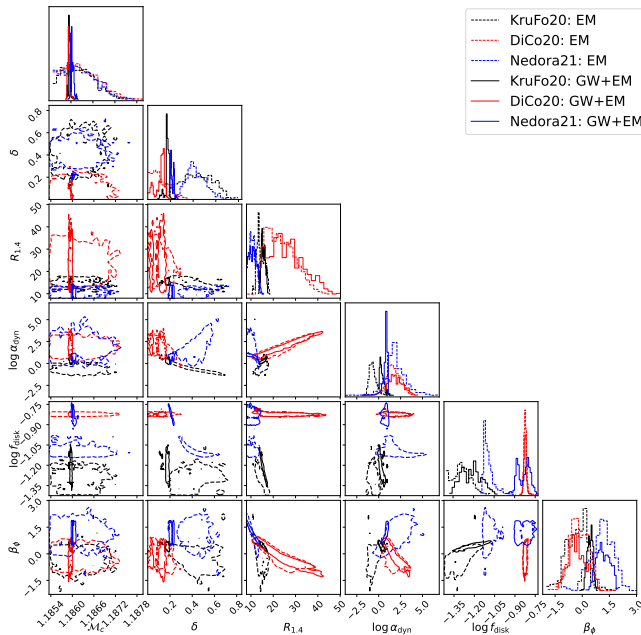
FIG. 5. Binary parameter posterior distributions using EM (dashed) and GW+EM (solid) likelihoods using $\log f_{\text{disk}}$ priors of [-0.9, -0.75], [-1.4, -1.2], and [-1.2, -1] for DiCo20, KruFo20, and Nedora21, respectively. The inclusion of the GW likelihood most noticeably affects the chirp mass $\mathcal{M}_c$ and mass asymmetry δ, while simultaneously providing tighter constraints on the neutron star radius $R_{1.4}$ and ejected disk fraction f_{disk} .

models prefer that the progenitor of AT2017gfo is a highly asymmetric binary ($\delta > 0$) with smaller NS radius $R_{1.4}$, with the DiCo20 models allowing equal-mass ($\delta = 0$) binaries with exceptionally large NS radius. Conversely, these inferences suggest that a surprisingly small fraction ($\sim 4-20\%$) of the expected disk mass is ejected as a wind, in contrast to most previous work [96, 97], but consistent with predictions from three-dimensional general relativistic, full transport neutrino radiation magnetohydrodynamics disk simulations [98].

B. Allowing no uncertainty in ejecta velocity ($\beta_\phi = 0$)

We perform an additional suite of studies in which we assume no systematic uncertainty in the v_{ej} predicted by the ejecta fits. For these analyses, we continue to treat f_{disk} as a free parameter. Despite the assumption of no velocity systematic uncertainty made in this section, the ejecta posteriors remain unchanged, behaving as in Figure 3. Thus, we still find that our kilonova model and subsequent EM likelihood provide the dominant constraint for the ejecta parameters.

However, without an additional parameter to encapsulate the ejecta systematics, we find several notable
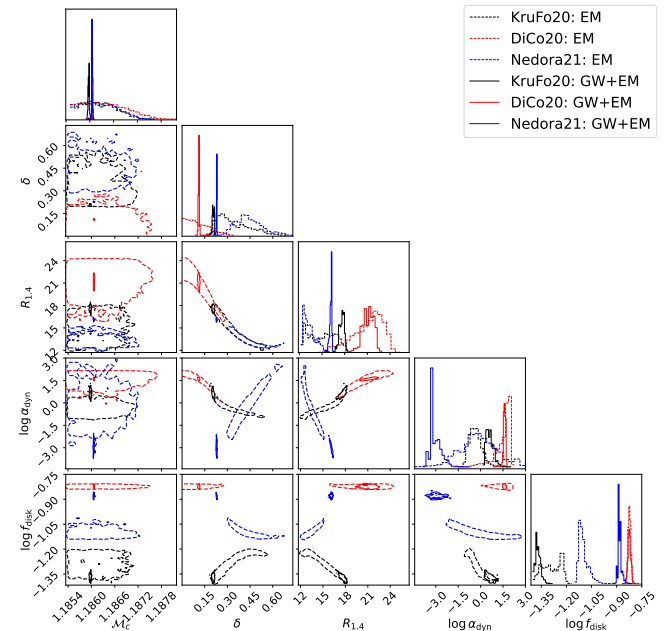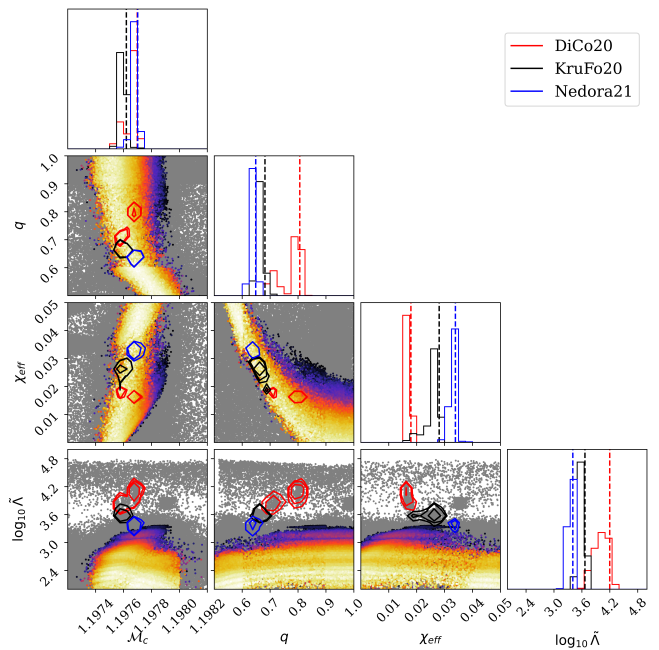

FIG. 6. Same as Figures 2 and 5, but not allowing for systematic uncertainty in v_d (i.e. $\beta_\phi = 0$). Note the recreation of the v_{ej} contours from Figure 1 in the $R_{1.4}$ vs. δ plane.

differences, largely dictated by the v_{ej} contours in Figure 1. Specifically, we find that for all three ejecta fits, the GW+EM analyses all favor large radii in order to replicate the low dynamical ejecta velocities necessitated by the $v_{\text{ej}} = v_d$ posteriors in Figure 3. Based on Figure 1, a tight constraint on v_{ej} requires either asymmetric NS at more conventional radius ($\delta \simeq 0.4$ and $R_{1.4} \simeq 15\text{km}$) or symmetric NS with extreme radius. Indeed, the union of all three $\delta - R_{1.4}$ posteriors in Figure 6 closely mirrors the underlying v_{ej} contours. As a result, this constraint

forces the posterior away from the peak GW likelihood, which favors lower NS radii and more symmetric binaries. In all three cases where we omit systematic error in velocity ($\beta_\phi = 0$), joint GW+EM inference mildly favors asymmetric binaries $\delta \simeq 0.1 - 0.2$ with large NS radius $R_{1.4} > 15$km.

C. Allowing no uncertainty in ejecta velocity and disk mass ejection fraction ($\beta_\phi = 0$ and $f_{\text{disk}} = 0.30$)

We also consider the case of a fixed disk mass ejection fraction, in which f_{disk} is not a free parameter, but restricted to the fixed value $f_{\text{disk}} = 30\%$. The purpose of this analysis is to evaluate the behavior of the ejecta fits in predicting light curves under the assumption of a generally applied ejected disk fraction. The top half of Figure 7 displays the same ejecta parameters as in Figure 3. While the dynamical mass m_{d} and viewing angle θ are somewhat consistent with prior results, the wind mass m_{w} and dynamical velocity v_{d} posteriors yield substantially different results. In the bottom half of Figure 7, we plot the light curves corresponding to the Nedora21 GW+EM posteriors shown in the top part of Figure 7. While the light curves corresponding to the median posterior values (solid lines) are clearly worse fits than those in Figure 4, the more striking feature lies in the exceptionally large uncertainties across all broadband filters. More specifically, the uncertainty bounds are much broader than before, resulting from the broad dynamic range of the m_{w} posteriors. The difficulty in constraining m_{w} comes from f_{disk} being directly tied to the amount of ejected wind mass; as such, what the m_w posteriors in Figure 7 are really showing us is the Monte Carlo integrator trying to reconcile the values of m_w that actually fit the data with the constricting value of f_{disk} = 30% that fixes the wind ejecta mass.

IV. DISCUSSION

We perform multimessenger inference of GW170817/AT2017gfo using three different ejecta models and a single kilonova model represented by the neural network surrogate provided in Ref. [52]. This surrogate, when compared with observations, leads to strong constraints on our kilonova model's observable parameters, with posterior extent likely comparable to the information extractable from a perfect model. While many systematic uncertainties have still yet to be incorporated into our analysis, many of which are well described in a recent study [55], our surrogate model is nevertheless sufficient to assess the prospects of, and challenges facing, multimessenger investigations. Thus, this surrogate provides us with an ideal opportunity to assess the consistency of and perform systematic uncertainty quantification of our methods to perform multimessenger inference, focusing on the remaining
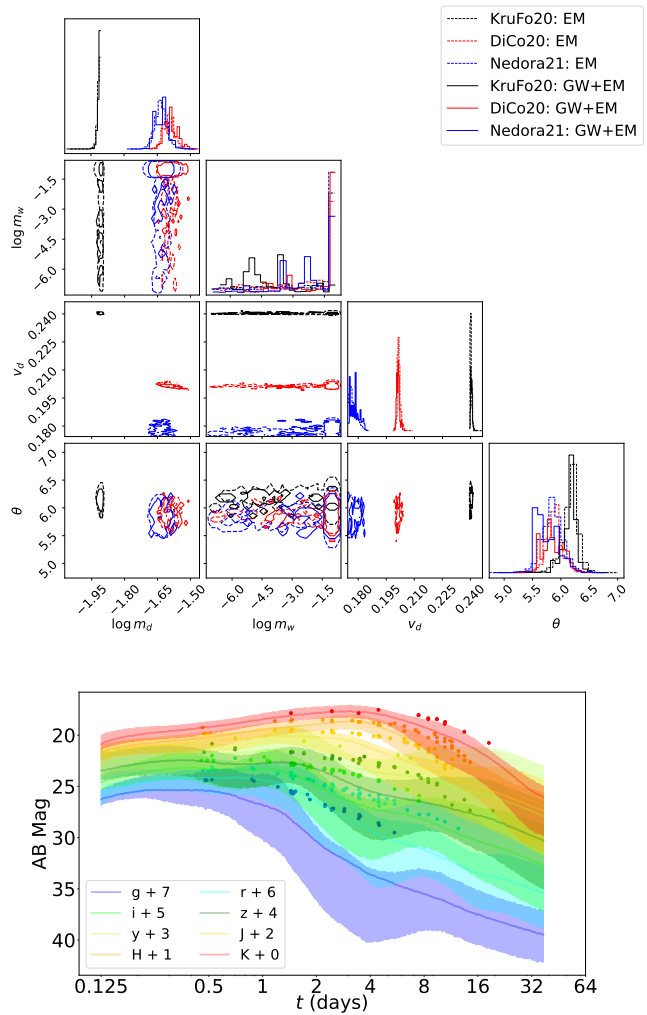

FIG. 7. *Top*: Ejecta posterior distributions using using EM (dashed) and GW+EM (solid) likelihoods with an assumed disk mass ejection of $f_{\text{disk}} = 30\%$. In contrast to Figure 3, m_w is less constrained (leading to the large uncertainties in the light curves below) and v_d is specific to the ejecta fit model. *Bottom*: Light curves associated with the Nedora21 GW+EM ejecta posteriors presented above, with solid lines corresponding to the median posterior values and shaded bands representing 1σ uncertainty. It is obvious that, at least for the purposes of parameter inference, assuming the same fixed disk fraction for all three ejecta fits yields poor fits to the data with a relatively high degree of uncertainty.

ingredients of that challenge. We find that the three ejecta fits we consider largely prefer asymmetric mass binaries (though one allows for symmetry), with all three ejecta fits encompassing effectively different regimes of the neutron star radius $R_{1.4}$.

Unsurprisingly, inference analyses using a joint EM and GW dataset are more constraining than using EM-only data. This behavior is most evident for the $\mathcal{M}_c$ and δ posteriors in Figure 5, which highlight the impact of including the gravitational likelihood $\mathcal{L}_{\text{GW}}$. The $\mathcal{M}_c$ posteriors for each fit clearly converge on a preferred

value when supplemented with GW information; likewise, the δ posteriors become narrower on both global (dynamic range of posterior values) and local (per-ejecta-fit posterior values) scales. With regard to the NS radius $R_{1.4}$ posteriors, the difference between EM and GW+EM analyses is less striking. More prevalent, however, are the different regions of the NS radius parameter space covered by the posteriors corresponding to each ejecta fit. Specifically, the GW+EM predictions for $R_{1.4}$ are roughly between 8–15 km, 10–20 km, and 10–40 km for the Nedora21 KruFo20 and DiCo20 forward models, respectively. These results strongly imply that, provided a constraining kilonova model, multimessenger inference about neutron star radius and, consequently, the dense matter equation of state is entirely dependent on the chosen forward model.

Keeping the relative impact of GW and EM information in mind, the joint GW/EM inferences shown in Figure 5 make sense. For almost all parameters, the addition of GW information only slightly perturbs the answers derived from EM information alone. This behavior is most evident in the bottom panel of Figure 5, where narrower priors on f_{disk} directly affect the ejected wind mass and thus the EM likelihood, shifting the δ and $R_{1.4}$ posteriors to better agreement across ejecta fits.

As explained in Section II A, we introduce the α_{dyn}, f_{disk}, and β_ϕ free parameters to quantify the systematic uncertainty of the ejecta fit predictions, with σ_{sys} encompassing all other sources of systematic uncertainty in our light curves. As previously mentioned, we do not plot σ_{sys} in Figure 5 because of its largely unconstrained and uninformative behavior. Conversely, Figure 5 shows that f_{disk} is the most constrained of these parameters, while the α_{dyn} posteriors are generally broader and show minimal preference across individual ejecta fits. The velocity systematics β_ϕ lie somewhere in between, with the Nedora and KruFo GW+EM analyses preferring slower velocities ($\beta_\phi > 0$) and the KruFo EM and DiCo analyses preferring faster velocities ($\beta_\phi < 0$). For the velocity values allowed by the range of β_ϕ, we find that, compared to the recovered value of $v_{\text{ej}} = v_{\text{d}} = 0.14$ from Figure 3, the KruFo20, DiCo20, and Nedora21 forward models recover relative uncertainties on the velocity of 30.7%, 138%, and 63%. For all but the KruFo20 fit, these relative differences are substantially higher than the 33% originally reported in Ref. [57] from which the ejecta velocity fits originate. Given the narrow peaks of the f_{disk} posteriors, we interpret the f_{disk} parameter as setting the scale for the wind ejecta mass, with the α_{dyn}, β_ϕ, and σ_{sys} parameters allowing our inference enough flexibility to fit the AT2017gfo light curves. Likewise, we expect the ejecta mass scale set by f_{disk} to be the dominant parameter determining the light curve behavior (see, e.g., [99]); however, recent studies have shown that velocity profiles can contribute significantly to variations in the light curves [100, 101]. Our velocity systematics can have substantial effects on inference, corroborating the findings of these recent studies. These results motivate more detailed studies of versatile ejecta fits which, among other effects, specifically focus on a separate treatment of dynamical and secular ejecta velocities.

Within the context of no velocity systematics ($\beta_\phi = 0$), a closer look at the $R_{1.4}$ vs. δ two-dimensional posterior in Figure 6 indicates a cubic relationship between the two parameters. Specifically, as the mass asymmetry of the binary increases $\delta \to 0.5$, the radius of the individual stars decreases $R_{1.4} \leftarrow 0$, indicating that more asymmetric binaries prefer a softer (more compressible) EOS. This behavior is exactly the same as that observed in Figure 1, where the ejecta velocity contours (dotted lines ranging from 0.1 to 0.2) dictated the $R_{1.4}$ vs. δ relationship. The persistence of this restrictive behavior from the naive contours in Figure 1 to our posteriors in Figure 6 strongly suggests that future analyses of the NS radius and EOS must include *both* mass and velocity systematic parameters, lest they introduce significant biases on top of the ones already present in selecting an ejecta forward model.

Finally, in the case where the fraction of ejected disk material is fixed to $f_{\text{disk}} = 30\%$, we recover low quality posteriors that clearly struggle to fit the data. Specifically, the wind mass m_{w} is unconstrained compared to the dynamical mass m_{d}, resulting in prohibitively large uncertainties in the light curves.

V. CONCLUSION

In this paper, we have examined multimessenger Bayesian inference of GW170817 and its kilonova AT2017gfo using forward-modeling ejecta predictions which are based on numerical relativity simulations of neutron star mergers. Using a fixed baseline kilonova model [52], we assess the impact of systematic uncertainty in ejecta modeling, using three forward model ejecta fits presented in Refs. [45–47]. We find that these three forward models are in tension with one another and necessarily over-constrain ejecta inference (i.e., they make more predictions than they have parameters). Using concrete interpretation of GW170817/AT2017gfo, and after adding a generous budget for systematic uncertainty above and beyond stated confidence, we illustrate the impact of the tension in these three models on multimessenger interpretation: we find distinctly different conclusions about the underlying binary with each ejecta model, even allowing for systematics. We furthermore point out that adopting stronger assumptions about ejecta, which omit one or more of our systematic uncertainty parameters, lead to even more extreme conclusions about AT2017gfo/GW170817.

Our study builds upon and extends work by [52], which emphasized purely phenomenological kilonova inference with a fiducial $\sigma_{\text{sys}} = 0.5$ or a similar prior on σ_{sys}, without ejecta forward modeling. Except for when we strongly limit our assumptions about ejecta systematics, our inferences about the observed kilonova ejecta are

identical.

We highlight that key elements of these models may be used well outside of their region of calibration (e.g., ejecta velocity) when used in conjunction with the surrogate kilonova model from our prior work in Ref. [52]. The primary observations highlighted by our analysis are:

- Fits to numerical relativity simulations of neutron star mergers which predict mass ejection suffer from systematic uncertainties stemming from the parameter coverage and accuracy of the simulations used to derive them. Unfortunately, multimessenger inference requires confidence in these predictions well outside conventional configurations, to confidently assess extreme scenarios.

- Given a kilonova model which can provide tight constraints on ejecta parameters, multimessenger inference about binary parameters like the neutron star radius and, consequently, the dense matter equation of state are strongly dependent on the chosen forward model and its ejecta predictions. The ejecta velocity in particular seems to have a strong impact, as ours and other contemporary inferences favor velocities at the low end of calibrated fits.

- Corroborating previous results (e.g. [100, 101]), we find that a treatment of *both* mass and velocity systematic uncertainties is required for maximally unbiased inference of ejecta forward model predictions.

- Within the context of our model, we find that the fraction of the ejected disk lies around $4 - 16\%$ for a GW170817-like event, with said fraction also dependent on the chosen forward model. This agrees with predictions from GRMHD simulations with full neutrino transport, but is in tension with assumptions typically made in the literature (up to 40% of disk ejection).

Our results suggest that there are currently no broadly applicable prescriptions which accurately map binary parameters to ejecta predictions or correctly assume the ejected fraction of an arbitrary post-merger accretion disk. The lack of such prescriptions strongly motivates future studies which examine the connection between numerical relativity simulations of neutron star mergers and their ejecta predictions. While future multimessenger observations of neutron star mergers will shed more light on the broader population of mergers, in the meantime, our conclusions suggest that significantly more additional numerical relativity studies are necessary to understand the connection between binary and ejecta parameters. Additionally, for kilonova models to be confidently used in multimessenger analyses such as the proof of concept presented in this manuscript, more work is required to improve the fidelity of the radiative transfer simulations used to model these events. Likewise, in understanding these connections, we encourage future studies to carefully consider the contexts within which each of the ejecta forward models is applicable and assume appropriate levels of uncertainty in their analyses.

VI.   ACKNOWLEDGMENTS

Appendix: Interpreting the DiCo20 $\tilde{\Lambda}$ Results

The DiCo20 $\tilde{\Lambda}$ and $R_{1.4}$ posteriors in Figures 2 and 5 are appreciably different from those corresponding to the KruFo20 and Nedora21 ejecta fits, favoring much larger radii and $\tilde{\Lambda}$ than informed by the GW likelihood. We examine the DiCo20 ejecta contours in Figure 8. The velocity prescription remains the same, while the disk mass and dynamical ejecta fits change. The dynamical ejecta contours behave similarly to the KruFo20 contours, with larger values of δ required to produce a higher quantity of dynamical ejecta. The disk mass contours (dashed lines) are the most different between the two fits. Whereas in the KruFo20 fits, disk mass was weakly dependent on δ and primarily set by $R_{1.4}$, the DiCo20 fits behave oppositely, with disk mass defined by δ and completely agnostic to $R_{1.4}$. This reversed dependency enables the DiCo20 posteriors to find solutions near $\delta = 0$ with low χ_{eff}, in line with the GW-informed likelihood; however, the lack of a $R_{1.4}$ constraint results in the uncharacteristically large $\tilde{\Lambda}$ values observed in Figure 2.

[1] B. P. Abbott, R. Abbott, T. D. Abbott, F. Acernese, K. Ackley, C. Adams, T. Adams, P. Addesso, R. X. Adhikari, V. B. Adya, C. Affeldt, M. Afrough, B. Agarwal, M. Agathos, K. Agatsuma, *et al.*, Phys. Rev. Lett. **119**,
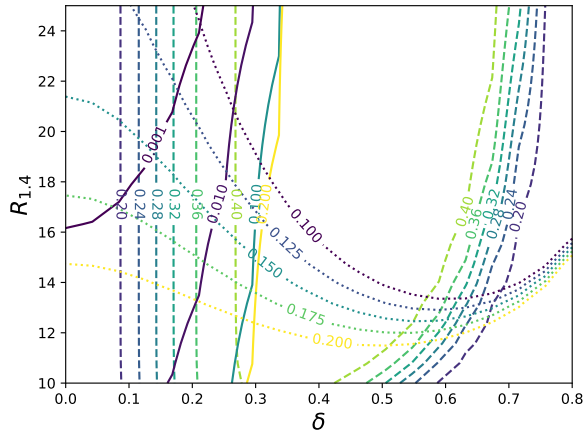
FIG. 8. Ejecta contours as in Figure 1, but for the DiCo20 forward model. The disk mass (dashed lines) is constrained by δ but unbounded in the $R_{1.4}$ dimension.

161101 (2017), arXiv:1710.05832 [gr-qc].

[2] B. P. Abbott, R. Abbott, T. D. Abbott, F. Acernese, K. Ackley, C. Adams, T. Adams, P. Addesso, R. X. Adhikari, V. B. Adya, C. Affeldt, M. Afrough, B. Agarwal, M. Agathos, K. Agatsuma, *et al.*, Astrophysical Journal Letters **848**, L12 (2017), arXiv:1710.05833 [astro-ph.HE].

[3] I. Andreoni, K. Ackley, J. Cooke, A. Acharyya, J. R. Allison, G. E. Anderson, M. C. B. Ashley, D. Baade, M. Bailes, K. Bannister, A. Beardsley, M. S. Bessell, F. Bian, P. A. Bland, M. Boer, *et al.*, PASA **34**, e069 (2017), arXiv:1710.05846 [astro-ph.HE].

[4] I. Arcavi, G. Hosseinzadeh, D. A. Howell, C. McCully, D. Poznanski, D. Kasen, J. Barnes, M. Zaltzman, S. Vasylyev, D. Maoz, and S. Valenti, Nature (London) **551**, 64 (2017).

[5] D. A. Coulter, R. J. Foley, C. D. Kilpatrick, M. R. Drout, A. L. Piro, B. J. Shappee, M. R. Siebert, J. D. Simon, N. Ulloa, D. Kasen, B. F. Madore, A. Murguia-Berthier, Y. C. Pan, J. X. Prochaska, E. Ramirez-Ruiz, *et al.*, Science **358**, 1556 (2017), arXiv:1710.05452 [astro-ph.HE].

[6] P. S. Cowperthwaite, E. Berger, V. A. Villar, B. D. Metzger, M. Nicholl, R. Chornock, P. K. Blanchard, W. Fong, R. Margutti, M. Soares-Santos, K. D. Alexander, S. Allam, J. Annis, D. Brout, D. A. Brown, *et al.*, Astrophysical Journal Letters **848**, L17 (2017), arXiv:1710.05840 [astro-ph.HE].

[7] M. C. Díaz, L. M. Macri, D. Garcia Lambas, C. Mendes de Oliveira, J. L. Nilo Castellón, T. Ribeiro, B. Sánchez, W. Schoenell, L. R. Abramo, S. Akras, J. S. Alcaniz, R. Artola, M. Beroiz, S. Bonoli, J. Cabral, *et al.*, Astrophysical Journal Letters **848**, L29 (2017), arXiv:1710.05844 [astro-ph.HE].

[8] M. R. Drout, A. L. Piro, B. J. Shappee, C. D. Kilpatrick, J. D. Simon, C. Contreras, D. A. Coulter, R. J. Foley, M. R. Siebert, N. Morrell, K. Boutsia, F. Di Mille, T. W. S. Holoien, D. Kasen, J. A. Kollmeier, *et al.*, Science **358**, 1570 (2017), arXiv:1710.05443 [astro-ph.HE].

[9] P. A. Evans, S. B. Cenko, J. A. Kennea, S. W. K. Emery, N. P. M. Kuin, O. Korobkin, R. T. Wollaeger, C. L. Fryer, K. K. Madsen, F. A. Harrison, *et al.*, Science **358**, 1565 (2017), https://www.science.org/doi/pdf/10.1126/science.aap9580.

[10] L. Hu, X. Wu, I. Andreoni, M. C. B. Ashley, J. Cooke, X. Cui, F. Du, Z. Dai, B. Gu, Y. Hu, H. Lu, X. Li, Z. Li, E. Liang, L. Liu, *et al.*, Science Bulletin **62**, 1433 (2017), arXiv:1710.05462 [astro-ph.HE].

[11] M. M. Kasliwal, E. Nakar, L. P. Singer, D. L. Kaplan, D. O. Cook, A. Van Sistine, R. M. Lau, C. Fremling, O. Gottlieb, J. E. Jencson, S. M. Adams, U. Feindt, K. Hotokezaka, S. Ghosh, D. A. Perley, *et al.*, Science **358**, 1559 (2017), arXiv:1710.05436 [astro-ph.HE].

[12] V. M. Lipunov, E. Gorbovskoy, V. G. Kornilov, N. Tyurina, P. Balanutsa, A. Kuznetsov, D. Vlasenko, D. Kuvshinov, I. Gorbunov, D. A. H. Buckley, A. V. Krylov, R. Podesta, C. Lopez, F. Podesta, H. Levato, *et al.*, Astrophysical Journal Letters **850**, L1 (2017), arXiv:1710.05461 [astro-ph.HE].

[13] E. Pian, P. D'Avanzo, S. Benetti, M. Branchesi, E. Brocato, S. Campana, E. Cappellaro, S. Covino, V. D'Elia, J. P. U. Fynbo, F. Getman, G. Ghirlanda, G. Ghisellini, A. Grado, G. Greco, *et al.*, Nature (London) **551**, 67 (2017), arXiv:1710.05858 [astro-ph.HE].

[14] S. J. Smartt, T. W. Chen, A. Jerkstrand, M. Coughlin, E. Kankare, S. A. Sim, M. Fraser, C. Inserra, K. Maguire, K. C. Chambers, M. E. Huber, T. Krühler, G. Leloudas, M. Magee, L. J. Shingles, *et al.*, Nature (London) **551**, 75 (2017), arXiv:1710.05841 [astro-ph.HE].

[15] N. R. Tanvir, A. J. Levan, C. González-Fernández, O. Korobkin, I. Mandel, S. Rosswog, J. Hjorth, P. D'Avanzo, A. S. Fruchter, C. L. Fryer, T. Kangas, B. Milvang-Jensen, S. Rosetti, D. Steeghs, R. T. Wollaeger, Z. Cano, C. M. Copperwheat, S. Covino, V. D'Elia, A. de Ugarte Postigo, P. A. Evans, W. P. Even, S. Fairhurst, R. Figuera Jaimes, C. J. Fontes, Y. I. Fujii, J. P. U. Fynbo, B. P. Gompertz, J. Greiner, G. Hodosan, M. J. Irwin, P. Jakobsson, U. G. Jørgensen, D. A. Kann, J. D. Lyman, D. Malesani, R. G. McMahon, A. Melandri, P. T. O'Brien, J. P. Osborne, E. Palazzi, D. A. Perley, E. Pian, S. Piranomonte, M. Rabus, E. Rol, A. Rowlinson, S. Schulze, P. Sutton, C. C. Thöne, K. Ulaczyk, D. Watson, K. Wiersema, and R. A. M. J. Wijers, Astrophysical Journal Letters **848**, L27 (2017), arXiv:1710.05455 [astro-ph.HE].

[16] E. Troja, L. Piro, H. van Eerten, R. T. Wollaeger, M. Im, O. D. Fox, N. R. Butler, S. B. Cenko, T. Sakamoto, C. L. Fryer, R. Ricci, A. Lien, R. E. Ryan, O. Korobkin, S. K. Lee, *et al.*, Nature (London) **551**, 71 (2017), arXiv:1710.05433 [astro-ph.HE].

[17] Y. Utsumi, M. Tanaka, N. Tominaga, M. Yoshida, S. Barway, T. Nagayama, T. Zenko, K. Aoki, T. Fujiyoshi, H. Furusawa, K. S. Kawabata, S. Koshida, C.-H. Lee, T. Morokuma, K. Motohara, *et al.*, PASJ **69**, 101 (2017), arXiv:1710.05848 [astro-ph.HE].

[18] S. Valenti, D. J. Sand, S. Yang, E. Cappellaro, L. Tartaglia, A. Corsi, S. W. Jha, D. E. Reichart, J. Haislip, and V. Kouprianov, Astrophysical Journal Letters **848**, L24 (2017).

[19] A. S. Pozanenko, M. V. Barkov, P. Y. Minaev, A. A. Volnova, E. D. Mazaeva, A. S. Moskvitin, M. A. Krugov, V. A. Samodurov, V. M. Loznikov, and M. Lyu-

tikov, Astrophysical Journal Letters **852**, L30 (2018), arXiv:1710.05448 [astro-ph.HE].

[20] L.-X. Li and B. Paczyński, Astrophysical Journal Letters **507**, L59 (1998).

[21] B. D. Metzger, G. Martínez-Pinedo, S. Darbha, E. Quataert, A. Arcones, D. Kasen, R. Thomas, P. Nugent, I. V. Panov, and N. T. Zinner, Monthly Notices of the Royal Astronomical Society **406**, 2650 (2010), arXiv:1001.5029 [astro-ph.HE].

[22] M. Shibata and K. Hotokezaka, Annual Review of Nuclear and Particle Science **69**, 41 (2019), arXiv:1908.02350 [astro-ph.HE].

[23] L. Piro, E. Troja, B. Zhang, G. Ryan, H. van Eerten, R. Ricci, M. H. Wieringa, A. Tiengo, N. R. Butler, S. B. Cenko, O. D. Fox, H. G. Khandrika, G. Novara, A. Rossi, and T. Sakamoto, Monthly Notices of the Royal Astronomical Society **483**, 1912 (2019), arXiv:1810.04664 [astro-ph.HE].

[24] A. Murguia-Berthier, E. Ramirez-Ruiz, F. De Colle, A. Janiuk, S. Rosswog, and W. H. Lee, Astrophys. J. **908**, 152 (2021), arXiv:2007.12245 [astro-ph.HE].

[25] S. Curtis, P. Bosch, P. Mösta, D. Radice, S. Bernuzzi, A. Perego, R. Haas, and E. Schnetter, Astrophysical Journal Letters **961**, L26 (2024), arXiv:2305.07738 [astro-ph.HE].

[26] The LIGO Scientific Collaboration, the Virgo Collaboration, B. P. Abbott, R. Abbott, T. D. Abbott, F. Acernese, K. Ackley, C. Adams, T. Adams, P. Addesso, and et al., Phys. Rev. Lett. **121**, 161101 (2018).

[27] M. Nicholl, B. Margalit, P. Schmidt, G. P. Smith, E. J. Ridley, and J. Nuttall, Monthly Notices of the Royal Astronomical Society **505**, 3016 (2021), arXiv:2102.02229 [astro-ph.HE].

[28] D. Kasen, B. Metzger, J. Barnes, E. Quataert, and E. Ramirez-Ruiz, Nature (London) **551**, 80 (2017), arXiv:1710.05463 [astro-ph.HE].

[29] F. K. Thielemann, M. Eichler, I. V. Panov, and B. Wehmeyer, Annual Review of Nuclear and Particle Science **67**, 253 (2017), arXiv:1710.02142 [astro-ph.HE].

[30] D. M. Siegel, European Physical Journal A **55**, 203 (2019), arXiv:1901.09044 [astro-ph.HE].

[31] K. Hotokezaka, K. Kyutoku, H. Okawa, M. Shibata, and K. Kiuchi, Phys. Rev. D **83**, 124008 (2011), arXiv:1105.4370 [astro-ph.HE].

[32] T. Dietrich, S. Bernuzzi, M. Ujevic, and W. Tichy, Phys. Rev. D **95**, 044045 (2017), arXiv:1611.07367 [gr-qc].

[33] D. Radice, A. Perego, K. Hotokezaka, S. A. Fromm, S. Bernuzzi, and L. F. Roberts, Astrophys. J. **869**, 130 (2018), arXiv:1809.11161 [astro-ph.HE].

[34] K. Kiuchi, K. Kyutoku, M. Shibata, and K. Taniguchi, Astrophysical Journal Letters **876**, L31 (2019), arXiv:1903.01466 [astro-ph.HE].

[35] A. Bauswein, S. Goriely, and H. T. Janka, Astrophys. J. **773**, 78 (2013), arXiv:1302.6530 [astro-ph.SR].

[36] V. Nedora, S. Bernuzzi, D. Radice, B. Daszuta, A. Endrizzi, A. Perego, A. Prakash, M. Safarzadeh, F. Schianchi, and D. Logoteta, Astrophys. J. **906**, 98 (2021), arXiv:2008.04333 [astro-ph.HE].

[37] T. Vincent, F. Foucart, M. D. Duez, R. Haas, L. E. Kidder, H. P. Pfeiffer, and M. A. Scheel, Phys. Rev. D **101**, 044053 (2020), arXiv:1908.00655 [gr-qc].

[38] Y. Sekiguchi, K. Kiuchi, K. Kyutoku, M. Shibata, and K. Taniguchi, Phys. Rev. D **93**, 124046 (2016), arXiv:1603.01918 [astro-ph.HE].

[39] K. Hotokezaka, K. Kiuchi, K. Kyutoku, H. Okawa, Y.-i. Sekiguchi, M. Shibata, and K. Taniguchi, Phys. Rev. D **87**, 024001 (2013), arXiv:1212.0905 [astro-ph.HE].

[40] L. Lehner, S. L. Liebling, C. Palenzuela, O. L. Caballero, E. O'Connor, M. Anderson, and D. Neilsen, Classical and Quantum Gravity **33**, 184002 (2016), arXiv:1603.00501 [gr-qc].

[41] A. Perego, S. Bernuzzi, and D. Radice, European Physical Journal A **55**, 124 (2019), arXiv:1903.07898 [gr-qc].

[42] V. Nedora, S. Bernuzzi, D. Radice, A. Perego, A. Endrizzi, and N. Ortiz, Astrophysical Journal Letters **886**, L30 (2019), arXiv:1907.04872 [astro-ph.HE].

[43] S. Bernuzzi, M. Breschi, B. Daszuta, A. Endrizzi, D. Logoteta, V. Nedora, A. Perego, D. Radice, F. Schianchi, F. Zappa, I. Bombaci, and N. Ortiz, Monthly Notices of the Royal Astronomical Society **497**, 1488 (2020), arXiv:2003.06015 [astro-ph.HE].

[44] Y. Sekiguchi, K. Kiuchi, K. Kyutoku, and M. Shibata, Phys. Rev. D **91**, 064059 (2015), arXiv:1502.06660 [astro-ph.HE].

[45] C. J. Krüger and F. Foucart, Phys. Rev. D **101**, 103002 (2020), arXiv:2002.07728 [astro-ph.HE].

[46] T. Dietrich, M. W. Coughlin, P. T. H. Pang, M. Bulla, J. Heinzel, L. Issa, I. Tews, and S. Antier, Science **370**, 1450 (2020), arXiv:2002.11355 [astro-ph.HE].

[47] V. Nedora, F. Schianchi, S. Bernuzzi, D. Radice, B. Daszuta, A. Endrizzi, A. Perego, A. Prakash, and F. Zappa, Classical and Quantum Gravity **39**, 015008 (2022), arXiv:2011.11110 [astro-ph.HE].

[48] E. M. Holmbeck, R. O'Shaughnessy, V. Delfavero, and K. Belczynski, Astrophys. J. **926**, 196 (2022), arXiv:2110.06432 [astro-ph.HE].

[49] P. T. H. Pang, T. Dietrich, M. W. Coughlin, M. Bulla, I. Tews, M. Almualla, T. Barna, R. W. Kiendrebeogo, N. Kunert, G. Mansingh, B. Reed, N. Sravan, A. Toivonen, S. Antier, R. O. VandenBerg, J. Heinzel, V. Nedora, P. Salehi, R. Sharma, R. Somasundaram, and C. Van Den Broeck, Nature Communications **14**, 8352 (2023), arXiv:2205.08513 [astro-ph.HE].

[50] G. Raaijmakers, S. Nissanke, F. Foucart, M. M. Kasliwal, M. Bulla, R. Fernández, A. Henkel, T. Hinderer, K. Hotokezaka, K. Lukošiūtė, T. Venumadhav, S. Antier, M. W. Coughlin, T. Dietrich, and T. D. P. Edwards, Astrophys. J. **922**, 269 (2021), arXiv:2102.11569 [astro-ph.HE].

[51] A. Henkel, F. Foucart, G. Raaijmakers, and S. Nissanke, Phys. Rev. D **107**, 063028 (2023), arXiv:2207.07658 [astro-ph.HE].

[52] Y. Peng, M. Ristić, A. Kedia, R. O'Shaughnessy, C. J. Fontes, C. L. Fryer, O. Korobkin, M. R. Mumpower, V. A. Villar, and R. T. Wollaeger, arXiv e-prints , arXiv:2402.05871 (2024), arXiv:2402.05871 [astro-ph.HE].

[53] C. L. Fryer, C. J. Fontes, O. Korobkin, M. Mumpower, R. Wollaeger, E. M. Holmbeck, and R. O'Shaugnessy, in *The Sixteenth Marcel Grossmann Meeting. On Recent Developments in Theoretical and Experimental General Relativity, Astrophysics, and Relativistic Field Theories*, edited by R. Ruffino and G. Vereshchagin (2023) pp. 1391–1404.

[54] M. R. Mumpower, T. M. Sprouse, J. M. Miller, K. A. Lund, J. C. Garcia, N. Vassh, G. C. McLaughlin, and R. Surman, Astrophys. J. **970**, 173 (2024), arXiv:2404.03699 [astro-ph.HE].

[55] D. Brethauer, D. Kasen, R. Margutti, and R. Chornock, Astrophys. J. **975**, 213 (2024), arXiv:2408.02731 [astro-ph.HE].

[56] A. Kedia, M. Ristić, R. O'Shaughnessy, A. B. Yelikar, R. T. Wollaeger, O. Korobkin, E. A. Chase, C. L. Fryer, and C. J. Fontes, Physical Review Research **5**, 013168 (2023), arXiv:2211.04363 [astro-ph.HE].

[57] T. Dietrich and M. Ujevic, Classical and Quantum Gravity **34**, 105014 (2017), arXiv:1612.03665 [gr-qc].

[58] M. W. Coughlin, T. Dietrich, Z. Doctor, D. Kasen, S. Coughlin, A. Jerkstrand, G. Leloudas, O. McBrien, B. D. Metzger, R. O'Shaughnessy, and S. J. Smartt, Monthly Notices of the Royal Astronomical Society **480**, 3871 (2018), arXiv:1805.09371 [astro-ph.HE].

[59] R. T. Wollaeger, C. L. Fryer, E. A. Chase, C. J. Fontes, M. Ristić, A. L. Hungerford, O. Korobkin, R. O'Shaughnessy, and A. M. Herring, The Astrophysical Journal **918**, 10 (2021).

[60] O. Korobkin, R. T. Wollaeger, C. L. Fryer, A. L. Hungerford, S. Rosswog, C. J. Fontes, M. R. Mumpower, E. A. Chase, W. P. Even, J. Miller, G. W. Misch, and J. Lippuner, Astrophys. J. **910**, 116 (2021).

[61] O. Just, V. Vijayan, Z. Xiong, S. Goriely, T. Soultanis, A. Bauswein, J. Guilet, H. T. Janka, and G. Martínez-Pinedo, Astrophysical Journal Letters **951**, L12 (2023), arXiv:2302.10928 [astro-ph.HE].

[62] R. T. Wollaeger and D. R. van Rossum, The Astrophysical Journal Supplement Series **214**, 28 (2014).

[63] C. Winteler, R. Käppeli, A. Perego, A. Arcones, N. Vasset, N. Nishimura, M. Liebendörfer, and F. K. Thielemann, Astrophysical Journal Letters **750**, L22 (2012).

[64] O. Korobkin, S. Rosswog, A. Arcones, and C. Winteler, Monthly Notices of the Royal Astronomical Society **426**, 1940 (2012).

[65] M. Reichert, C. Winteler, O. Korobkin, A. Arcones, J. Bliss, M. Eichler, U. Frischknecht, C. Fröhlich, R. Hirschi, M. Jacobi, J. Kuske, G. Martínez-Pinedo, D. Martin, D. Mocelj, T. Rauscher, and F. K. Thielemann, Astroph. J. S. **268**, 66 (2023), arXiv:2305.07048 [astro-ph.IM].

[66] M. Reichert, C. Winteler, O. Korobkin, A. Arcones, J. Bliss, M. Eichler, U. Frischknecht, C. Fröhlich, R. Hirschi, M. Jacobi, J. Kuske, G. Martínez-Pinedo, D. Martin, D. Moclj, T. Rauscher, and F.-K. Thielemann, WinNet: v1.0.1, Zenodo (2023).

[67] J. Barnes, D. Kasen, M.-R. Wu, and G. Martínez-Pinedo, The Astrophysical Journal **829**, 110 (2016).

[68] R. T. Wollaeger, O. Korobkin, C. J. Fontes, S. K. Rosswog, W. P. Even, C. L. Fryer, J. Sollerman, A. L. Hungerford, D. R. van Rossum, and A. B. Wollaber, Monthly Notices of the Royal Astronomical Society **478**, 3298 (2018), https://academic.oup.com/mnras/article-pdf/478/3/3298/25067894/sty1018.pdf.

[69] C. J. Fontes, H. L. Zhang, J. Abdallah Jr., R. E. H. Clark, D. P. Kilcrease, J. Colgan, R. T. Cunningham, P. Hakel, N. H. Magee, and M. E. Sherrill, Journal of Physics B Atomic Molecular Physics **48**, 144014 (2015).

[70] C. J. Fontes, C. L. Fryer, A. L. Hungerford, R. T. Wollaeger, and O. Korobkin, Monthly Notices of the Royal Astronomical Society **493**, 4143 (2020).

[71] Y. Ralchenko, K. Olsen, C. J. Fontes, C. L. Fryer, A. L. Hungerford, R. T. Wollaeger, and O. Korobkin, NIST-LANL Lanthanide Opacity Database (ver. 1.2), [Online]. Available: https://nlte.nist.gov/OPAC [Apr 11 2023] 10.18434/mds2-2375 (2023).

[72] M. Ristić, E. Champion, R. O'Shaughnessy, R. Wollaeger, O. Korobkin, E. A. Chase, C. L. Fryer, A. L. Hungerford, and C. J. Fontes, Physical Review Research **4**, 013046 (2022), arXiv:2105.07013 [astro-ph.HE].

[73] B. J. Shappee, J. D. Simon, M. R. Drout, A. L. Piro, N. Morrell, J. L. Prieto, D. Kasen, T. W. S. Holoien, J. A. Kollmeier, D. D. Kelson, D. A. Coulter, R. J. Foley, C. D. Kilpatrick, M. R. Siebert, B. F. Madore, A. Murguia-Berthier, Y. C. Pan, J. X. Prochaska, E. Ramirez-Ruiz, A. Rest, C. Adams, K. Alatalo, E. Bañados, J. Baughman, R. A. Bernstein, T. Bitsakis, K. Boutsia, J. R. Bravo, F. Di Mille, C. R. Higgs, A. P. Ji, G. Maravelias, J. L. Marshall, V. M. Placco, G. Prieto, and Z. Wan, Science **358**, 1574 (2017), arXiv:1710.05432 [astro-ph.HE].

[74] N. R. Tanvir, A. J. Levan, C. González-Fernández, O. Korobkin, I. Mandel, S. Rosswog, J. Hjorth, P. D'Avanzo, A. S. Fruchter, C. L. Fryer, T. Kangas, B. Milvang-Jensen, S. Rosetti, D. Steeghs, R. T. Wollaeger, *et al.*, Astrophysical Journal Letters **848**, L27 (2017), arXiv:1710.05455 [astro-ph.HE].

[75] The LIGO Scientific Collaboration, the Virgo Collaboration, B. P. Abbott, R. Abbott, T. D. Abbott, F. Acernese, K. Ackley, C. Adams, T. Adams, P. Addesso, and et al., Physical Review X **9**, 011001 (2019), arXiv:1805.11579 [gr-qc].

[76] The LIGO Scientific Collaboration, the Virgo Collaboration, B. P. Abbott, R. Abbott, T. D. Abbott, S. Abraham, F. Acernese, K. Ackley, C. Adams, V. B. Adya, *et al.*, Classical and Quantum Gravity **37**, 045006 (2020).

[77] A. Kedia, R. O'Shaughnessy, L. Wade, and A. Yelikar, arXiv e-prints , arXiv:2405.17326 (2024), arXiv:2405.17326 [astro-ph.HE].

[78] A. Vilkha, A. Yelikar, R. O'Shaughnessy, and J. Read, in prep (2024).

[79] J. Lange, R. O'Shaughnessy, and M. Rizzo, Submitted to PRD; available at arxiv:1805.10457 (2018).

[80] D. Wysocki, R. O'Shaughnessy, J. Lange, and Y.-L. L. Fang, Phys. Rev. D **99**, 084026 (2019), arXiv:1902.04934 [astro-ph.IM].

[81] J. Wofford, A. B. Yelikar, H. Gallagher, E. Champion, D. Wysocki, V. Delfavero, J. Lange, C. Rose, V. Valsan, S. Morisaki, J. Read, C. Henshaw, and R. O'Shaughnessy, Phys. Rev. D **107**, 024040 (2023).

[82] A. Kedia, R. O'Shaughnessy, L. Wade, and A. Yelikar, Submitted to PRD, available as arxiv:2405.17326 (2024).

[83] T. Narikawa, N. Uchikata, K. Kawaguchi, K. Kiuchi, K. Kyutoku, M. Shibata, and H. Tagoshi, Phys. Rev. Res. **2**, 043039 (2020).

[84] E. E. Flanagan and T. Hinderer, Phys. Rev. D **77**, 021502 (2008), arXiv:0709.1915 [astro-ph].

[85] T. Dietrich, S. Khan, R. Dudi, S. J. Kapadia, P. Kumar, A. Nagar, F. Ohme, F. Pannarale, A. Samajdar, S. Bernuzzi, G. Carullo, W. Del Pozzo, M. Haney, C. Markakis, M. Pürrer, G. Riemenschneider, Y. E. Setyawati, K. W. Tsang, and C. Van Den Broeck, Phys. Rev. D **99**, 024029 (2019).

[86] T. Dietrich, A. Samajdar, S. Khan, N. K. Johnson-McDaniel, R. Dudi, and W. Tichy, Phys. Rev. D **100**, 044003 (2019).

[87] R. Abbott, T. D. Abbott, S. Abraham, F. Acernese, K. Ackley, C. Adams, R. X. Adhikari, V. B. Adya, C. Affeldt, M. Agathos, and et al., SoftwareX **13**, 100658 (2021), arXiv:1912.11716 [gr-qc].

[88] The LIGO Scientific Collaboration, The Virgo Collaboration, B. P. Abbott, R. Abbott, T. D. Abbott, F. Acernese, K. Ackley, C. Adams, T. Adams, P. Addesso, and et al., Physical Review X **9**, 031040 (2019).

[89] L. S. Collaboration, Parameter estimation sample release for gwtc-1 (2018).

[90] K. Hotokezaka, E. Nakar, O. Gottlieb, S. Nissanke, K. Masuda, G. Hallinan, K. P. Mooley, and A. T. Deller, Nature Astronomy **3**, 940 (2019), arXiv:1806.10596 [astro-ph.CO].

[91] K. P. Mooley, E. Nakar, K. Hotokezaka, G. Hallinan, A. Corsi, D. A. Frail, A. Horesh, T. Murphy, E. Lenc, D. L. Kaplan, K. de, D. Dobie, P. Chandra, A. Deller, O. Gottlieb, M. M. Kasliwal, S. R. Kulkarni, S. T. Myers, S. Nissanke, T. Piran, C. Lynch, V. Bhalerao, S. Bourke, K. W. Bannister, and L. P. Singer, Nature (London) **554**, 207 (2018), arXiv:1711.11573 [astro-ph.HE].

[92] J. Wofford, A. B. Yelikar, H. Gallagher, E. Champion, D. Wysocki, V. Delfavero, J. Lange, C. Rose, V. Valsan, S. Morisaki, J. Read, C. Henshaw, and R. O'Shaughnessy, Phys. Rev. D **107**, 024040 (2023).

[93] V. Tiwari, C. Hoy, S. Fairhurst, and D. MacLeod, Phys. Rev. D **108**, 023001 (2023), arXiv:2303.01463 [astro-ph.HE].

[94] K. Kawaguchi, S. Fujibayashi, M. Shibata, M. Tanaka, and S. Wanajo, Astrophys. J. **913**, 100 (2021), arXiv:2012.14711 [astro-ph.HE].

[95] M. Ristić, R. O'Shaughnessy, V. A. Villar, R. T. Wollaeger, O. Korobkin, C. L. Fryer, C. J. Fontes, and A. Kedia, Physical Review Research **5**, 043106 (2023), arXiv:2304.06699 [astro-ph.HE].

[96] D. Radice, S. Bernuzzi, and A. Perego, Annual Review of Nuclear and Particle Science **70**, 95 (2020), arXiv:2002.03863 [astro-ph.HE].

[97] S. Fujibayashi, M. Shibata, S. Wanajo, K. Kiuchi, K. Kyutoku, and Y. Sekiguchi, Phys. Rev. D **101**, 083029 (2020), arXiv:2001.04467 [astro-ph.HE].

[98] J. M. Miller, B. R. Ryan, J. C. Dolence, A. Burrows, C. J. Fontes, C. L. Fryer, O. Korobkin, J. Lippuner, M. R. Mumpower, and R. T. Wollaeger, Phys. Rev. D **100**, 023008 (2019), arXiv:1905.07477 [astro-ph.HE].

[99] M. Ristić, R. O'Shaughnessy, V. A. Villar, R. T. Wollaeger, O. Korobkin, C. L. Fryer, C. J. Fontes, and A. Kedia, Physical Review Research **5**, 043106 (2023), arXiv:2304.06699 [astro-ph.HE].

[100] D. Tak, Z. L. Uhm, and J. H. Gillanders, Astrophys. J. **958**, 121 (2023), arXiv:2310.15608 [astro-ph.HE].

[101] C. L. Fryer, A. L. Hungerford, R. T. Wollaeger, J. M. Miller, S. De, C. J. Fontes, O. Korobkin, A. Kedia, M. Ristić, and R. O'Shaughnessy, Astrophys. J. **961**, 9 (2024), arXiv:2311.05005 [astro-ph.HE].